

## Fabrication and optical properties of large-scale arrays of gold nanocavities based on rod-in-a-tube coaxials

A. Murphy, Y. Sonnefraud, A. V. Krasavin, P. Ginzburg, F. Morgan et al.

Citation: *Appl. Phys. Lett.* **102**, 103103 (2013); doi: 10.1063/1.4794935

View online: <http://dx.doi.org/10.1063/1.4794935>

View Table of Contents: <http://apl.aip.org/resource/1/APPLAB/v102/i10>

Published by the [American Institute of Physics](#).

---

### Related Articles

Atomic structure of tensile-strained GaAs/GaSb(001) nanostructures

*Appl. Phys. Lett.* **102**, 102105 (2013)

The induction of nanographitic phase on Fe coated diamond films for the enhancement in electron field emission properties

*J. Appl. Phys.* **113**, 094305 (2013)

Note: Size effects on the tensile response of top-down fabricated Si nanobeams

*Rev. Sci. Instrum.* **84**, 036102 (2013)

Double-sided tin nanowire arrays for advanced thermal interface materials

*Appl. Phys. Lett.* **102**, 093105 (2013)

Controlled growth of vertical ZnO nanowires on copper substrate

*Appl. Phys. Lett.* **102**, 083105 (2013)

---

### Additional information on *Appl. Phys. Lett.*

Journal Homepage: <http://apl.aip.org/>

Journal Information: [http://apl.aip.org/about/about\\_the\\_journal](http://apl.aip.org/about/about_the_journal)

Top downloads: [http://apl.aip.org/features/most\\_downloaded](http://apl.aip.org/features/most_downloaded)

Information for Authors: <http://apl.aip.org/authors>

## ADVERTISEMENT

**JANIS** Does your research require low temperatures? Contact Janis today.  
Our engineers will assist you in choosing the best system for your application.



10 mK to 800 K      LHe/LN<sub>2</sub> Cryostats  
Cryocoolers      Magnet Systems  
Dilution Refrigerator Systems  
Micro-manipulated Probe Stations

[sales@janis.com](mailto:sales@janis.com)      [www.janis.com](http://www.janis.com)  
Click to view our product web page.

## Fabrication and optical properties of large-scale arrays of gold nanocavities based on rod-in-a-tube coaxials

A. Murphy,<sup>1,a)</sup> Y. Sonnefraud,<sup>2</sup> A. V. Krasavin,<sup>3</sup> P. Ginzburg,<sup>3</sup> F. Morgan,<sup>1</sup> J. McPhillips,<sup>1,b)</sup> G. Wurtz,<sup>3</sup> S. A. Maier,<sup>2</sup> A. V. Zayats,<sup>3</sup> and R. Pollard<sup>1</sup>

<sup>1</sup>Centre for Nanostructured Media, Queen's University Belfast, Belfast BT7 1NN, United Kingdom

<sup>2</sup>Experimental Solid State Group, Department of Physics, Imperial College London, London SW7 2AZ, United Kingdom

<sup>3</sup>Department of Physics, King's College London, Strand, London WC2R 2LS, United Kingdom

(Received 7 January 2013; accepted 25 February 2013; published online 12 March 2013)

Centimeter sized arrays of gold coaxial rod-in-a tube cavities have been fabricated using anodized aluminum oxide as a template. The etching process used to create the cavities enables the production of extremely small gaps between tube and rod, on the order of 5 nm, smaller than those created by standard fabrication techniques. Normal incidence spectroscopy reveals two extinction peaks in the visible and near infrared wavelength range associated with resonant plasmonic modes excited in the structure. Numerical simulations show that the modes are associated with in-phase and out-of-phase hybridization of transverse dipolar excitations in the nanorod and in the tube.

© 2013 American Institute of Physics. [<http://dx.doi.org/10.1063/1.4794935>]

The field of nanotechnology relies on the continuous development of nanostructures with exceptional properties and tailored functionalities not found in conventional bulk materials. To make further advancements in nanotechnology and all related fields, it is necessary to simplify and scale up the methods by which nanostructures are assembled. Over the past decades, several methods have been developed for creating nanostructured arrays with porous alumina templates,<sup>1-3</sup> electron beam lithography,<sup>4</sup> nanosphere lithography,<sup>5</sup> and nanoimprint lithography,<sup>6</sup> to name a few. Some of these processes are reaching a saturation point, where they can no longer meet demands for reducing nanostructure dimensions and overall cost-effectiveness. Therefore, innovative schemes and techniques need to be developed for the realization of new types of nano-architectures, with designed optical functionalities.

Noble metal nanostructures, having unique optical properties including a negative permittivity in the visible and infrared regime, receive ever-increasing attention in the field of plasmonics, a thriving branch of nanophotonics. They have the ability to confine light beyond the diffraction limit due to the excitation of free electron oscillations at their surfaces, known as surface plasmons.<sup>7-9</sup> In the field of nonlinear optics, plasmonic nanostructures are of particular interest with their exceptional ability to enhance and focus incident electromagnetic energy to deep sub-wavelength dimensions, which is a key advantage as many nonlinear phenomena are proportional to higher powers of the local electromagnetic field amplitude.<sup>10</sup> The most commonly exploited of the many promising applications emerging from extraordinary local field enhancement are surface enhanced Raman scattering (SERS) for single molecule detection<sup>11</sup> and plasmon enhanced second harmonic generation

(SHG).<sup>12,13</sup> Bright localized surface plasmon (LSP) resonances also manifest in the far-field as peaks in optical extinction whose wavelength is highly dependent on the refractive index of the surrounding medium. This has resulted in the extensive use of metallic nanostructures as highly sensitive label-free plasmonic biosensors.<sup>14,15</sup>

A vast range of metallic nanostructures have been designed in an attempt to tailor and tune localised surface plasmon resonances.<sup>16,17</sup> Recent advancements in chemistry have resulted in the synthesis of nanospheres,<sup>18</sup> nanorods,<sup>19</sup> nanoshells,<sup>20</sup> and even more complex geometries in solution. Developments in top-down and template-assisted methods has resulted in the growth of large scale nanostructured arrays including nanorods,<sup>21</sup> nanotubes,<sup>22</sup> and nanoholes.<sup>23</sup> Here, we bring this approach to an advanced technological level, presenting a method for the scalable production of arrays of gold coaxial rod-tube nanocavities with exceptionally small gap dimensions on the order of 5 nm, which exceeds other current fabrication capabilities. Using far-field spectroscopy, reinforced by numerical modeling, we reveal that the optical properties of the structure are defined by hybridized transverse resonances supported by individual coaxial rod-tube particles.

The coaxial rod-tube (CRT) cavity arrays are fabricated using a porous alumina oxide template fixed to a glass substrate and following the step by step procedure presented in Fig. 1.<sup>21,22</sup> In brief, a planar aluminum film is deposited onto a glass substrate by magnetron sputtering, the thickness of which determines the maximum possible height of the nanostructures. The aluminum film is anodized (Fig. 1(a)), the barrier layer is removed by sodium hydroxide (NaOH) etching and gold nanorods are electrodeposited into the pores onto a sputtered gold under layer (Fig. 1(b)).<sup>23</sup> NaOH is then used to etch a shell around the gold nanorods (Fig. 1(c)) into which the sacrificial conjugated polymer, polypyrrole, is deposited (Fig. 1(d)). A second shell is etched around the hybrid polymer/gold structure (Fig. 1(e)) in which the gold tube is finally deposited to form the CRT (Fig. 1(f)). The

<sup>a)</sup>Author to whom correspondence should be addressed. Electronic mail: antony.murphy@qub.ac.uk

<sup>b)</sup>Author's present address: FEI Company, Europe NanoPort, Achtseweg Noord 5, Bldg, 5651 GG Eindhoven, The Netherlands.

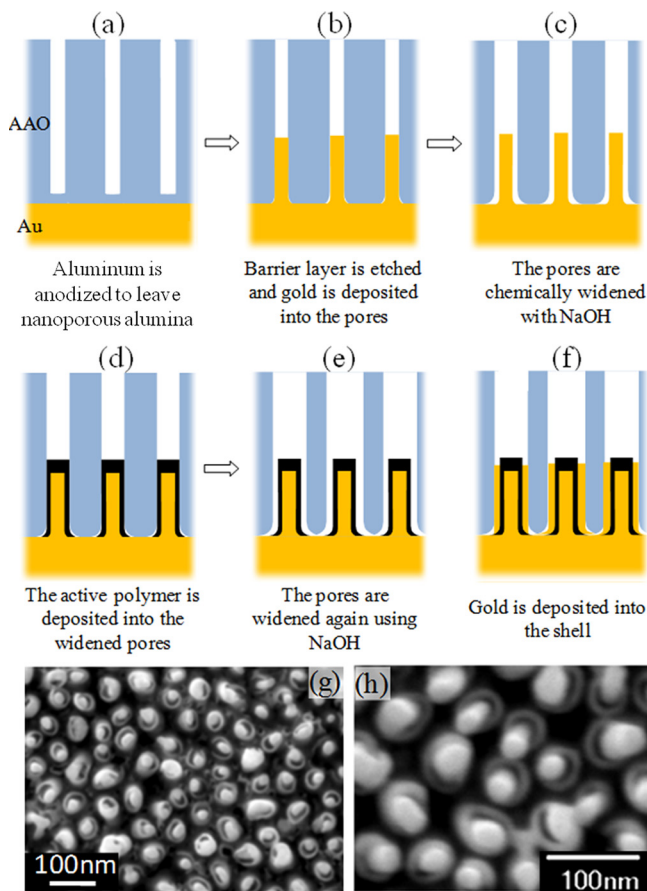


FIG. 1. (a)–(f) Schematic showing the process for fabricating gold coaxial rod-tube arrays. (g) and (h) SEM images of the final structure after polypyrrole and alumina removal. The average dimensions (and standard deviation,  $\sigma$ ) of the structures in (h) are: 20 nm nanorod diameter ( $\sigma = 3$  nm), 10 nm nanotube wall ( $\sigma = 1$  nm), 7.5 nm cavity ( $\sigma = 1$  nm), and 70 nm spacing ( $\sigma = 6$  nm).

polymer in the gap between the tube and the rod as well as the alumina matrix can be removed using a combination of plasma and NaOH etch to reveal the final structure in Figs. 1(g) and 1(h). Further details on the fabrication procedure can be found elsewhere.<sup>24</sup>

TABLE I. The geometrical tunability of the coaxial nanostructures.

Tunable parameter	Method of tuning	Dimensions (nm)
Spacing	Anodisation voltage	50–80
Height	Electrodeposition time	0–400
Inner rod diameter	1st NaOH etch time	20–30
Cavity thickness	2nd NaOH etch time	5–15
Nanotube wall thickness	3rd NaOH etch time	5–15

The fabrication route described in Fig. 1 for creating CRT arrays results in excellent geometrical tunability (Table I). The outer diameter of the structures is limited by the centre-to-centre spacing, which is set by the anodisation voltage. It is possible to extend the spacing further using oxalic or phosphoric acids for anodization.<sup>25</sup> The height of the structures is controlled by varying the electrodeposition times and is only limited by the alumina template thickness ( $\sim 400$  nm in this case). Thus, the height of the core or outer shell can be tuned independently. In Fig. 1, the core is higher than the outer shell: once the polypyrrole and alumina are removed, the cores can lean to the side, which explains the non-concentric aspect of the structures. The lateral dimensions are controlled using NaOH etching parameters (time and concentration) and can result in gaps between the wire and the tube in the 5 nm range, essentially acting as a tunable plasmonic cavity. This cavity size exceeds current fabrication capabilities, including e-beam and nanoimprint methods, and is made in a much simpler, cheaper, and scalable way.

The plasmonic behavior of CRT arrays was studied using normal incidence transmission spectroscopy.<sup>24</sup> The illumination conditions are suitable to the excitation of all the bright eigenmodes of the structures, coupled to plane waves. The average dimensions taken from Fig. 1(h) of the structure were as follows: 20 nm nanorod diameter ( $\sigma = 3$  nm), 10 nm nanotube wall ( $\sigma = 1$  nm), 7.5 nm cavity ( $\sigma = 1$  nm), 150 nm in height, and 70 nm spacing ( $\sigma = 6$  nm). Fig. 2(a) shows that the CRT arrays exhibit two extinction peaks around 540 nm and 800 nm (black curve). Finite element modeling (FEM) of the same structure using bulk gold dielectric function<sup>26</sup> agrees with experimental results with two peaks observed at similar wavelengths (red curve). The model produces sharper resonances as it uses average values for the experimentally inhomogeneous structure dimensions and higher quality gold dielectric function than electrodeposited gold.<sup>27</sup>

Electric field distributions of the modeled structure are presented in Figs. 2(b) and 2(c), for its component along the polarization direction of the incident light, and for the resonances at 525 nm and 810 nm. It appears that those resonances are transversal resonances of distinct symmetry. The charge distributions at the top surface of the structure are highlighted in (d) and (e). The picture is similar to what is observed in the case of thin concentric disk-ring cavities.<sup>28,29</sup> The low energy mode (at 810 nm) is a bonding mode formed from the hybridization of the lowest order transverse dipole of the tube and the wire. Those two dipoles are antiparallel in the CRT cavities (Fig. 2(e)). On the other

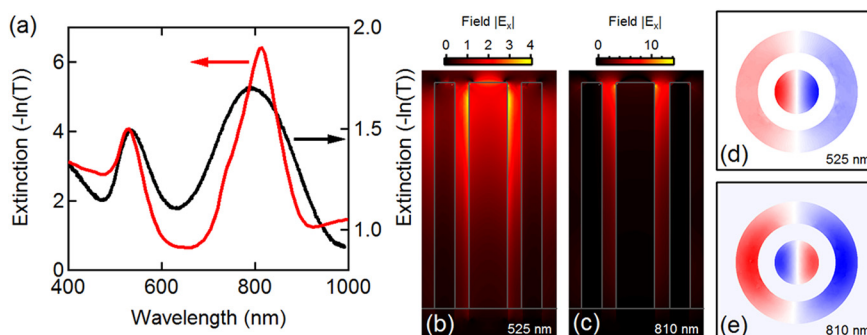


FIG. 2. (a) Experimental (black) and modeled (red) normal incidence extinction ( $-\ln(\text{Transmission})$ ) spectra of a gold coaxial rod-tube array surrounded by the alumina matrix. (b) and (c) longitudinal cross section of the  $|E_x|$  component of the field along the polarization direction, for 525 and 810 nm incident wavelengths respectively. (d) and (e) charge distribution at the top surface of the CRT, at 525 and 810 nm wavelengths, respectively. Red and blue indicate opposite polarity of the charges.

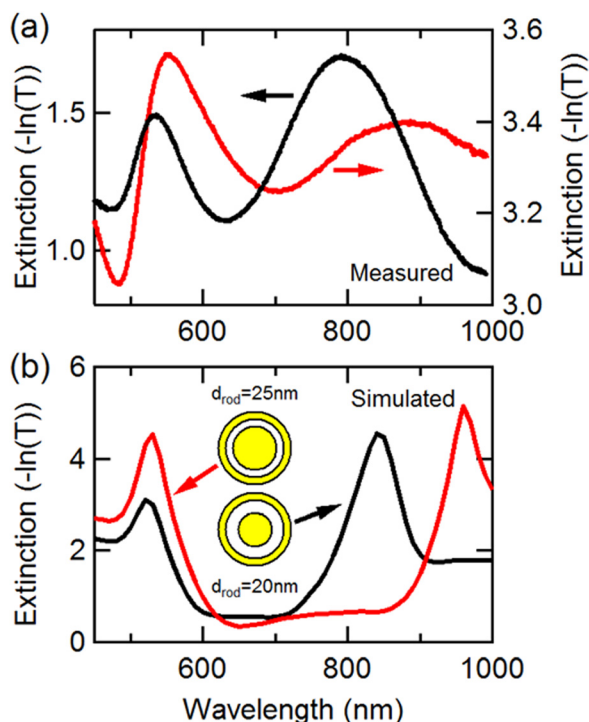


FIG. 3. (a) Optical tunability of the system was carried out by changing the diameter of the inner rod from 20 nm (black) to 25 nm (red). (b) Simulated optical response of the system when increasing nanorod diameter from 20 nm (black) to 25 nm (red).

hand, in the higher order resonance (at 525 nm) the dipoles are oriented in the same direction—the interaction is antibonding.<sup>20</sup>

The geometry of the coaxial structure can be easily tuned by altering the three NaOH etch times. Such tuning was demonstrated by varying the inner rod diameter whilst retaining the overall outer diameter. This was achieved experimentally by varying the first etch time (30–60 s) and adjusting the subsequent etches to keep the overall etch time constant (90 s). Fig. 3 presents the extinction spectra corresponding to two different structures. The diameter of the inner rods increased from 20 nm (black curve) to 25 nm (red curve) by increasing the etch time, the outer diameter being approximately 50 nm for both. The longer wavelength peak is very sensitive to the dimension of the inner rod, red-shifting by more than 100 nm for this 5 nm increase in the rod's diameter. On the other hand, the shorter wavelength peak shows weak tunability with diameter, red-shifting by only 20 nm. Simulations show that by increasing the inner rod diameter further, the bonding resonance can be tuned

further into the infrared regime. The structure can therefore be tailored for non-linear processes,<sup>30–32</sup> like second harmonic generation, where the resonances enhance both the fundamental (500 nm) and second harmonic (1000 nm) modes simultaneously.

We finish our discussion by investigating the potential of using this nanostructure as a plasmonic biosensor.<sup>14</sup> Finite element modeling is again used to simulate the effects of varying the refractive index of the medium surrounding the CRT arrays. The refractive index ( $n$ ) was varied from 1.3 to 1.5, which approximates the range for different concentrations of adsorbing protein layers.<sup>33</sup> A comparative study of the structures sensitivity was carried out by exposing either the cavity or the outer walls independently to changes in refractive index, or the full structure. The extinction obtained in the case where the full environment is changed is plotted in Fig. 4(a). Both extinction peaks experience a spectral redshift when the surrounding refractive index is increased, and a similar behavior is observed when only the cavity or the space between the outer walls sees a refractive index change. The bulk sensitivity ( $m$ ) of the structure can be determined from the following:

$$m = \frac{\Delta\lambda_{peak}}{\Delta n},$$

where  $\lambda_{peak}$  is the peak wavelength of the resonance for each refractive index,  $n$ . And the figure of merit (FOM) of the sensitivity of the resonance is defined as the bulk sensitivity divided by the full width at half maximum of the resonance.<sup>34</sup> Fig. 4(b) presents the shift of the low energy peak with the change of refractive index. The sensitivity  $m$  is extracted from linear fits to those trends. When the complete environment is changed, the peak at 520 nm shows a lower sensitivity to changes in refractive index with a shift of 30 nm/RIU (refractive index unit). In contrast, simulations show that the peak at 820 nm is an order of magnitude more sensitive with a predicted sensitivity of 400 nm/RIU, comparable to the best plasmonic refractive index sensors based on localized plasmon resonances. The FWHM in the simulations is 90 nm, which results in a FOM of 4.5. The resonance observed in experiments is much broader with an equivalent FWHM of approximately 200 nm. This would reduce the FOM of this nanostructure to  $\sim 2$ . Although the structures have a broad resonance, they cover a very large area of the sample, and this advantage might compensate for the inconvenience of the lower FOM even for sensing applications.

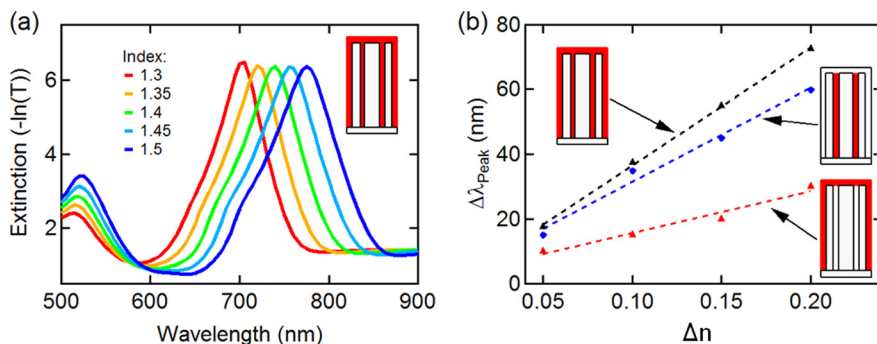


FIG. 4. (a) Simulated refractive index sensing characteristics of the coaxial nanostructures. It is tested by varying the surrounding refractive index ( $n$ ) from 1.3 (red curve) to 1.5 (dark blue curve) in steps of 0.05. (b) The bulk sensitivity of the complete coaxial structure (black line) to refractive index changes compared to only exposing the cavity (blue) and outer walls (red) for the lower energy (bonding) peak.

The bulk sensitivity of the coaxial rod-tube cavities compares favorably with other alumina based biosensors including nanowires ( $m \approx 280 \text{ nm/RIU}$ ,  $\text{FOM} = 1.7$ ),<sup>35</sup> nanotubes ( $m \approx 250 \text{ nm/RIU}$ ,  $\text{FOM} = 2.5$ )<sup>14</sup> and is not far from the one for single particle sensing with concentric disk-ring nanocavities ( $m \approx 600 \text{ nm/RIU}$ ,  $\text{FOM} = 3$ ).<sup>28</sup> The cavity is the most sensitive part of the structure, showing a bulk sensitivity of  $300 \text{ nm/RIU}$  compared to  $120 \text{ nm/RIU}$  for the outer walls only. This result is in contrast for the behavior of gold nanotubes where the plasmonic modes are localized to the outer walls, which makes them most sensitive to changes in refractive index.<sup>14,22</sup> The coaxial structure is particularly exciting for biosensing as the highly sensitive cavity can be tuned to accept small molecules (in the range of 5–15 nm) whilst the outer walls of the structure can simultaneously detect larger molecules. The fact that the modes can also be excited at normal incidence by unpolarized light means a simple detection system can be employed making it a commercially viable substrate for biosensing.

In conclusion, we have presented a method to produce concentric rod-tube cavities, using templates of aluminum oxide. The geometry of the structures can be controlled precisely by changing the conditions of growth. Gaps in the 5 nm range can be obtained which can be filled in by a spacing material that can be chosen to achieve specific properties (gain, non-linearities), and benefit from the large field enhancement provided by the structures. The structures exhibit two extinction peaks, which originate from resonances corresponding to in-phase and out-of-phase hybridization of dipolar transverse excitations in the wire and in the tube. These structures are cheap to produce on large surfaces and could constitute cost effective substrates for field enhancement and sensing.

The fabrication route gives excellent tunability over the nanostructure dimensions, which means the resonant plasmonic modes can be tuned across the visible and near infrared spectrum. The tunability of the structure is not just limited to the dimensions, as it is possible to deposit a wide range of metals, semiconductors, and polymers into alumina pores.<sup>36–39</sup> For example, the possibility of creating a nickel core/gold tube structure is of particular interest as it is promising for magneto-plasmonic applications.<sup>40–42</sup> Because of the relatively strong field confinement the cavity can sustain, the CRT geometry may also offer practical solutions in the design of active devices, both at the nanoscale and the macroscale with the use of an active spacer medium for light amplification,<sup>43</sup> nonlinear optical properties,<sup>31</sup> or light harvesting in solar cells.<sup>44</sup>

More generally, the fabricated structures could serve as excellent platforms for the realization of integrated nonlinear optical components. As an outlook for here, we point out several promising approaches for the achievement of strong nonlinear effects. First, nonlinear polymers could be deposited between the tube and its core, where the local electromagnetic field reaches its maximum. The robustness of the fabrication together with a precise control over the resonance locations enables to achieve structures resonant at both first and second harmonics, dramatically increasing the efficiency for second-harmonic generation processes.<sup>12</sup> Moreover, huge nonlinearities could also emerge from the metal interfaces,

as was recently proposed.<sup>45</sup> Similar approaches, relying on the resonance spectra matching, could be applied to SERS.

The authors would like to acknowledge the EPSRC Active Plasmonics Programme Grant for funding and support. Y.S. acknowledges support from the Leverhulme trust. P.G. acknowledges the Royal Society for International Newton Fellowship.

<sup>1</sup>C. A. Foss, Jr., G. L. Hornyak, J. A. Stockert, and C. R. Martin, *J. Phys. Chem.* **98**, 2963–2971 (1994).

<sup>2</sup>H. Masuda and K. Fukuda, *Science* **268**, 1466 (1995).

<sup>3</sup>H. Masuda and M. Satoh, *Jpn. J. Appl. Phys., Part 1* **35**, 126–129 (1996).

<sup>4</sup>Y.-W. Su, C.-S. Wu, C.-C. Chen, and C.-D. Chen, *Adv. Mater.* **15**, 49 (2003).

<sup>5</sup>C. L. Cheung, R. J. Nikolic, C. E. Reinhardt, and T. F. Wang, *Nanotechnology* **17**, 1339 (2006).

<sup>6</sup>S. Y. Chou, P. R. Krauss, W. Zhang, L. Guo, and L. Zhuang, *J. Vac. Sci. Technol. B* **15**(6), 2897–2904 (1997).

<sup>7</sup>S. A. Maier, *Plasmonics: Fundamentals and Applications* (Springer, New York, 2007).

<sup>8</sup>W. L. Barnes, A. Dereux, and T. W. Ebbesen, *Nature* **424**, 824 (2003).

<sup>9</sup>V. Giannini, A. I. Fernández-Domínguez, Y. Sonnefraud, T. Roschuk, R. Fernández-García, and S. A. Maier, *Small* **6**, 2498 (2010).

<sup>10</sup>M. Kauranen and A. V. Zayats, *Nature Photon.* **6**, 737–748 (2012).

<sup>11</sup>S. M. Nie and S. R. Emory, *Science* **275**, 1102–1106 (1997).

<sup>12</sup>Y. Pu, R. Grange, C. Hsieh, and D. Psaltis, *Phys. Rev. Lett.* **104**, 207402 (2010).

<sup>13</sup>H. Aouani, M. Navarro-Cia, M. Rahmani, T. P. Sidiropoulos, M. Hong, R. F. Oulton, and S. A. Maier, *Nano Lett.* **12**, 4997–5002 (2012).

<sup>14</sup>J. McPhillips, A. Murphy, M. P. Jonsson, W. R. Hendren, R. Atkinson, F. Höök, A. V. Zayats, and R. J. Pollard, *ACS Nano* **4**(4), 2210–2216 (2010).

<sup>15</sup>A. B. Dahlin, J. O. Tegenfeldt, and F. Hook, *Anal. Chem.* **78**, 4416–4423 (2006).

<sup>16</sup>N. Berkovitch, P. Ginzburg, and M. Orenstein, *J. Phys.: Condens. Matter* **24**, 073202 (2012).

<sup>17</sup>Y. Sonnefraud, A. L. Koh, D. W. McComb, and S. A. Maier, *Laser Photonics Rev.* **6**, 277 (2012).

<sup>18</sup>Y. Sun and Y. Xia, *Science* **298**(5601), 2176–2179 (2002).

<sup>19</sup>Y.-Y. Yu, S.-S. Chang, C.-L. Lee, and C. R. Wang, *J. Phys. Chem. B* **101**(34), 6661–6664 (1997).

<sup>20</sup>E. Prodan, C. Radloff, N. J. Halas, and P. Nordlander, *Science* **302**(5644), 419–422 (2003).

<sup>21</sup>R. Atkinson, W. R. Hendren, G. A. Wurtz, W. Dickson, A. V. Zayats, P. Evans, and R. J. Pollard, *Phys. Rev. B* **73**, 235402 (2006).

<sup>22</sup>A. Murphy, J. McPhillips, W. Hendren, C. McClatchey, R. Atkinson, G. Wurtz, A. V. Zayats, and R. J. Pollard, *Nanotechnology* **22**(4), 045705 (2011).

<sup>23</sup>A. G. Brolo, R. Gordon, B. Leathem, and K. L. Kavanagh, *Langmuir* **20**, 4813–4815 (2004).

<sup>24</sup>See supplementary material at <http://dx.doi.org/10.1063/1.4794935> for further details on the fabrication procedure for creating the coaxial nanostructured arrays.

<sup>25</sup>P. Evans, W. R. Hendren, R. Atkinson, G. A. Wurtz, W. Dickson, A. V. Zayats, and R. J. Pollard, *Nanotechnology* **17**, 5746–5753 (2006).

<sup>26</sup>P. B. Johnson and R. W. Christy, *Phys. Rev. B* **6**, 4370–4379 (1972).

<sup>27</sup>R. J. Pollard, A. Murphy, W. R. Hendren, P. R. Evans, R. Atkinson, G. A. Wurtz, A. V. Zayats, and V. A. Podolskiy, *Phys. Rev. Lett.* **102**, 127405 (2009).

<sup>28</sup>F. Hao, P. Nordlander, Y. Sonnefraud, P. Van Dorpe, and S. A. Maier, *ACS Nano* **3**, 643–652 (2009).

<sup>29</sup>Y. Sonnefraud, N. Verellen, H. Sobhani, G. A. E. Vandenbosch, V. V. Moshchalkov, P. Van Dorpe, P. Nordlander, and S. A. Maier, *ACS Nano* **4**(3), 1664–1670 (2010).

<sup>30</sup>P. Ginzburg, A. Nevet, N. Berkovitch, A. Normatov, G. M. Lerman, A. Yanai, U. Levy, and M. Orenstein, *Nano Lett.* **11**, 220–224 (2011).

<sup>31</sup>G. A. Wurtz, R. Pollard, W. Hendren, G. P. Wiederrecht, D. J. Gosztola, V. A. Podolskiy, and A. V. Zayats, *Nat. Nanotechnol.* **6**(2), 107–111 (2011).

<sup>32</sup>W. Dickson, G. A. Wurtz, P. Evans, D. O'Connor, R. Atkinson, R. Pollard, and A. V. Zayats, *Phys. Rev. B* **76**, 115411 (2007).

- <sup>33</sup>J. Voros, *Biophys. J.* **87**, 553–561 (2004).
- <sup>34</sup>L. J. Sherry, S.-H. Chang, G. C. Schatz, and R. P. Van Duyne, *Nano Lett.* **5**(10), 2034–2038 (2005).
- <sup>35</sup>H. Chen, X. Kou, Z. Yang, W. Ni, and J. Wang, *Langmuir* **24**, 5233–5237 (2008).
- <sup>36</sup>R.-L. Zong, J. Zhou, Q. Li, B. Du, B. Li, M. Fu, X.-W. Qi, L.-T. Li, and S. Buddhudu, *J. Phys. Chem. B* **108**(43), 16713–16716 (2004).
- <sup>37</sup>K. Nielsch, R. B. Wehrspohn, J. Barthel, J. Kirschner, U. Gosele, S. F. Fischer, and H. Kronmuller, *Appl. Phys. Lett.* **79**(9), 1360–1362 (2001).
- <sup>38</sup>C. H. Liu, J. A. Zapien, Y. Yao, X. M. Meng, C. S. Lee, S. S. Fan, Y. Lifshitz, and S. T. Lee, *Adv. Mater.* **15**(10), 38–841 (2003).
- <sup>39</sup>Y. Cao and T. E. Mallouk, *Chem. Mater.* **20**(16), 5260–5265 (2008).
- <sup>40</sup>P. R. Evans, W. R. Hendren, R. Atkinson, and R. J. Pollard, *J. Electrochem. Soc.* **154**(9), K79–K82 (2007).
- <sup>41</sup>V. V. Temnov, G. Armelles, U. Woggon, D. Guzatov, A. Cebollada, A. Garcia-Martin, J.-M. Garcia-Martin, T. Thomay, A. Leitenstorfer, and R. Bratschitsch, *Nature Photon.* **4**, 107–111 (2010).
- <sup>42</sup>P. K. Jain, Y. Xiao, R. Walsworth, and A. E. Cohen, *Nano Lett.* **9**(4), 1644–1650 (2009).
- <sup>43</sup>M. A. Noginov, G. Zhu, A. M. Belgrave, R. Bakker, V. M. Shalaev, E. E. Narimanov, S. Stout, E. Herz, T. Suteewong, and U. Wiesner, *Nature* **460**, 1110–1112 (2009).
- <sup>44</sup>V. E. Ferry, L. A. Sweatlock, D. Pacifici, and H. A. Atwater, *Nano Lett.* **8**(12), 4391–4397 (2008).
- <sup>45</sup>P. Ginzburg, A. Krasavin, Y. Sonnefraud, A. Murphy, R. Pollard, S. A. Maier, and A. V. Zayats, *Phys. Rev. B* **86**, 085422 (2012).